Journal of The Electrochemical Society, **150** (12) G849-G853 (2003)
0013-4651/2003/150(12)/G849/5/$7.00 © The Electrochemical Society, Inc.

Characteristics of ZrO_2 Films with Al and Pt Gate Electrodes

Seok-Woo Nam,[a] Jung-Ho Yoo,[a] Suheun Nam,[a] Dae-Hong Ko,[a,z] Cheol-Woong Yang,[b] and Ja-Hum Ku[c]

[a]*Department of Ceramic Engineering, Yonsei University, Seodaemoon-ku, Seoul 120-749, Korea*
[b]*School of Metallurgical and Materials Engineering, Sungkyunkwan University, Jangan-gu, Suwon 440-746, Korea*
[c]*Samsung Electronics Company, Limited, Semiconductor Research and Development Division, Kyunggi-do, Korea*

We investigated interfacial stabilities of ZrO_2 films with Al and Pt electrodes formed by magnetron sputtering upon annealing and consequent changes of their metal-oxide-semiconductor capacitor characteristics. The as-deposited ZrO_2 films deposited using a sputtering power of 300 W were amorphous, while after annealing in N_2 at 600°C for 5 min the films became polycrystalline with a mixture of monoclinic and tetragonal phases. After the deposition of electrodes, we found that the amorphous interlayer which is presumed to be Al_2O_3 was formed at the ZrO_2/Al interface, while platinum (Pt) electrodes showed no interlayer at the interface with ZrO_2 films. The value of the capacitance equivalent thickness for the ZrO_2 film with the Al electrode was larger than that of the case with the Pt electrode by about 12 Å, which is due to the presence of the additional Al_2O_3 interlayer at the Al/ZrO_2 interface. The capacitance-voltage measurement showed that the difference in flatband voltage (V_{FB}) between the ZrO_2 films and the two different electrodes is about 1.2 V, which is due to the work function difference between the two electrode materials.
© 2003 The Electrochemical Society. [DOI: 10.1149/1.1624843] All rights reserved.

Manuscript submitted December 2, 2002; revised manuscript received June 13, 2003. Available electronically November 5, 2003.

Silicon dioxide has been used as the gate dielectric material in metal oxide semiconductor field effect transistor (MOSFET) devices for over 40 years. The conventional SiO_2 dielectrics, however, showed the issue of direct tunneling of carriers in the sub-2.0 nm thickness regime, which results in significant leakage current flowing through the SiO_2 layer.[1-3] Therefore, the fabrication of the sub-0.1 μm MOSFET devices requires the development of new gate dielectric materials with lower leakage current levels than SiO_2 at the same equivalent oxide thickness values. Alternative dielectric materials, such as Si_3N_4, Si_3N_4/SiO_2 stack,[4-8] Y_2O_3,[9] Al_2O_3,[10] TiO_2,[11,12] Ta_2O_5,[13-16] $SrTiO_3$, and $(Ba_xSr_{1-x})TiO_3$[17,18] have been suggested as candidate materials. These materials, however, have demonstrated issues of low dielectric constant values or poor thermal stability with Si substrates.[11-18] Recently, ZrO_2,[19-21] HfO_2,[22,23] and their silicates[24,25] have been considered as promising alternative gate dielectric materials due to their high dielectric constant values and good thermal stabilities with Si substrates.[26]

Among the key issues related to the high-*k* gate stack such as gate poly depletion effects or boron penetration,[27] is interfacial instability in direct contact with gate electrode materials as well as with Si substrates. In particular, the interfacial reactions between electrodes and high-*k* oxides affect the electrical properties of complementary metal-oxide semiconductor (CMOS) devices such as decrease of the effective capacitance values. Therefore, good thermal stability with gate electrodes must be acquired in order to be employed as gate dielectrics. In this paper we report on the stability of sputtered ZrO_2 films in contact with two different gate electrode materials of Al and Pt, which are generally used for the evaluation of metal-oxide-semiconductor (MOS) capacitor structures.

Experimental

p-Type silicon(100) wafers with a resistivity of 8-15 Ω cm were cleaned by the RCA cleaning method and then the native oxide was removed with a 1% HF solution. The ZrO_2 films were prepared via the reactive dc magnetron sputtering method from a Zr metal target with a 99.9% purity in the Ar + O_2 gas ambients. The sputtering was performed at room temperature with a power of 300 W. The system was initially pumped down to 2×10^{-7} Torr and the pressure during sputtering maintained at 6×10^{-3} Torr with an O_2 flow rate of 5.4 sccm ($Ar/O_2 = 5$). The substrate underwent a 4 rpm rotation for the uniformity of deposited films. Postdeposition annealing (PDA) by furnace in a N_2 ambient was performed at 600°C for 5 min. Postannealing by furnace in either an O_2 or N_2 ambients was performed at 700-800°C for 10 min. Al and Pt were deposited as the top electrode materials. The top electrodes of Al and Pt films were prepared using the dc magnetron sputtering method from Al and Pt metal targets with 99.9% purity in the Ar gas ambient. Sputtering was performed at room temperature with 100 W power.

The thickness of the deposited films was confirmed by ellipsometry or X-ray reflectometry. Microstructures of both the films and the interfaces between the electrodes and the films were characterized and compared by a cross-sectional transmission electron microscopy (TEM) and an X-ray photoelectron spectroscopy (XPS). For XPS data acquisition, Al Kα radiation (1486.6 eV) was used as photon source and the analysis chamber was maintained at 5×10^{-9} Torr. All experimental scans were performed at a constant pass energy of 23.5 eV and a constant takeoff angle of 45°. In addition, the XPS spectra were all obtained at room temperature before and after Ar ion sputtering. For the Ar ion sputtering we used an ion energy of 3 keV and a beam current density of 1.5×10^{-5} A/cm^2.

Capacitance-voltage (C-V) characteristics of MOS structures with ZrO_2 films with Al or Pt electrodes were measured using an HP4284A. The area of the MOS (Al/ZrO_2/Si or Pt/ZrO_2/Si) capacitors was about 1.1×10^{-4} cm^2. The capacitance equivalent thickness (CET) was calculated from the accumulation capacitance at 1 MHz, and quantum mechanical effect was not considered. The gate bias sweeping was from +2 to −4 V for the C-V measurement.

Results and Discussion

The thicknesses of the as-deposited and annealed ZrO_2 films were measured by high-resolution TEM (HRTEM). Figure 1 shows the cross-sectional HRTEM micrographs of the ZrO_2 films on Si substrates after deposition and after annealing at 600°C for 5 min in an N_2 ambient. The physical thicknesses of the ZrO_2 films were measured to be about 9-10 nm for both films. The as-deposited film is amorphous (see Fig. 1a) and changes to its crystalline phase after annealing (see Fig. 1b). The annealed ZrO_2 films show the crystalline lattice fringes having spacing of about 2.94 Å that corresponds to the (101) plane of the tetragonal ZrO_2 phase. In order to identify the crystalline structures of annealed films, we examined the samples by plan-view diffraction pattern analysis. The plan-view diffraction pattern in Fig. 1c demonstrated that the film consists of monoclinic and tetragonal ZrO_2 phases. Notably, an interfacial

[z] E-mail: dhko@yonsei.ac.kr

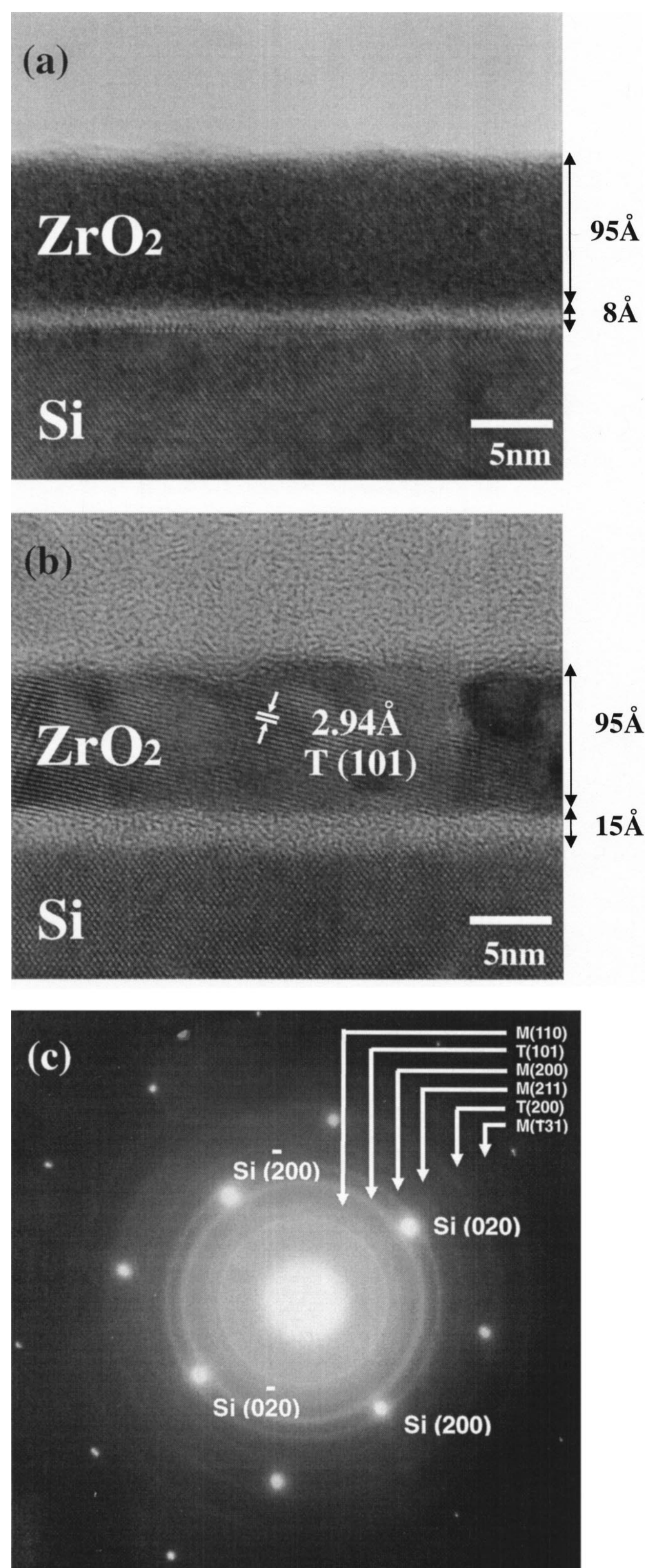

Figure 1. Cross-sectional HRTEM micrographs of (a) as-deposited ZrO_2 film and (b) postannealed ZrO_2 film at 600°C in N_2 for 5 min. (c) Plan-view diffraction pattern image of postannealed ZrO_2 film at 600°C in N_2 for 5 min.

amorphous layer is clearly observed between the ZrO_2 films and the Si substrates in the HRTEM image. The thickness of the interface layer was measured to be about 8 Å in the as-deposited sample and it increased to about 15 Å after annealing. As reported in our previous publications, the growth of the oxide layer is due to the oxidation of the substrate by the diffusion of oxidizing species from the ambient through the ZrO_2 film.[28] Similar results were observed in the CeO_2 films[29] and the Y_2O_3 films[30] deposited on Si substrates.

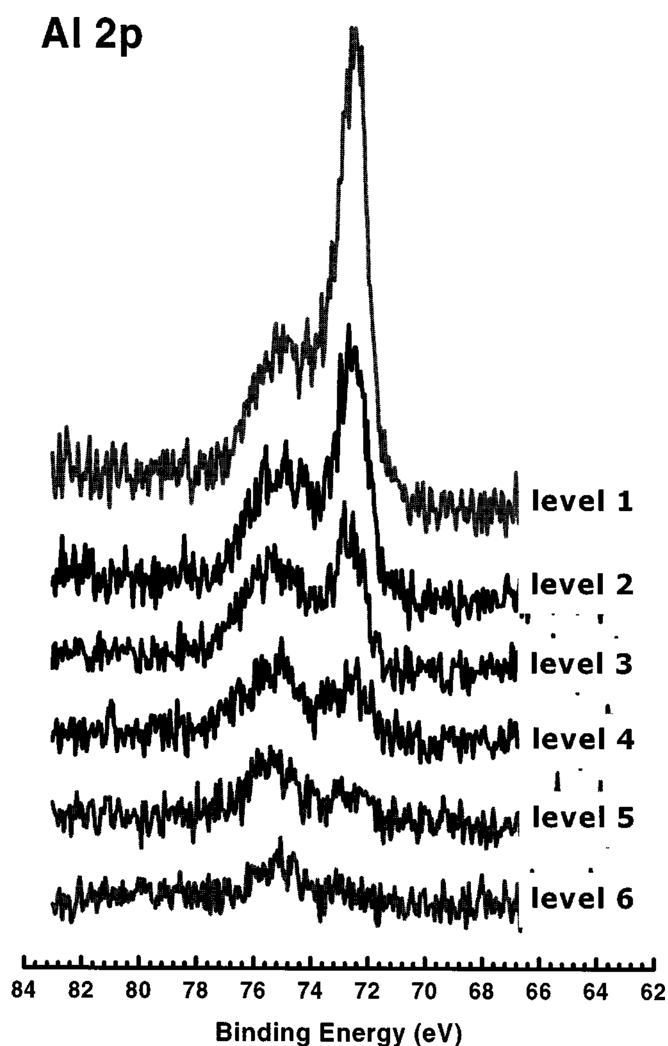

Figure 2. Al 2p signal in XPS spectra for ZrO_2 film with Al top electrode.

Al electrodes and Pt electrodes were deposited on ZrO_2 films by dc magnetron sputtering. The microstructures of the interfaces between the electrodes and the oxide films were analyzed by XPS and HRTEM. In order to investigate the interfacial reactions in the $Al/ZrO_2/Si$ and the $Pt/ZrO_2/Si$ systems, the chemical binding states at the Al/ZrO_2 and Pt/ZrO_2 interface were analyzed by XPS. For the XPS analysis, 10 nm thick $Al/ZrO_2/Si$ and 10 nm thick $Pt/ZrO_2/Si$ gate stacks were fabricated and annealed under the same annealing conditions. Initially, 10 nm thick Al and Pt films were etched to Al/ZrO_2 and Pt/ZrO_2 interface by Ar sputtering in an XPS chamber, after which spectra for Al 2p, Pt 4f, Zr 3d, and O 1s were obtained at each etching step from the Al/ZrO_2 and Pt/ZrO_2 interface to the Si substrate. Figure 2 illustrates the changes of the Al 2p signal in XPS spectra as the Al electrode was etched (level 1 meaning Al/ZrO_2 and level 6 meaning ZrO_2). The peaks with binding energy corresponding to photoelectrons in metallic Al (72.9 eV) as well as with higher binding energies were observed at the Al/ZrO_2 interfaces. Detailed XPS spectra at stage 4 are shown in Fig. 3a. The Al 2p binding energy for the metallic Al and the binding energy of 75.5 eV are clearly shown in the spectra, which demonstrates the pres-

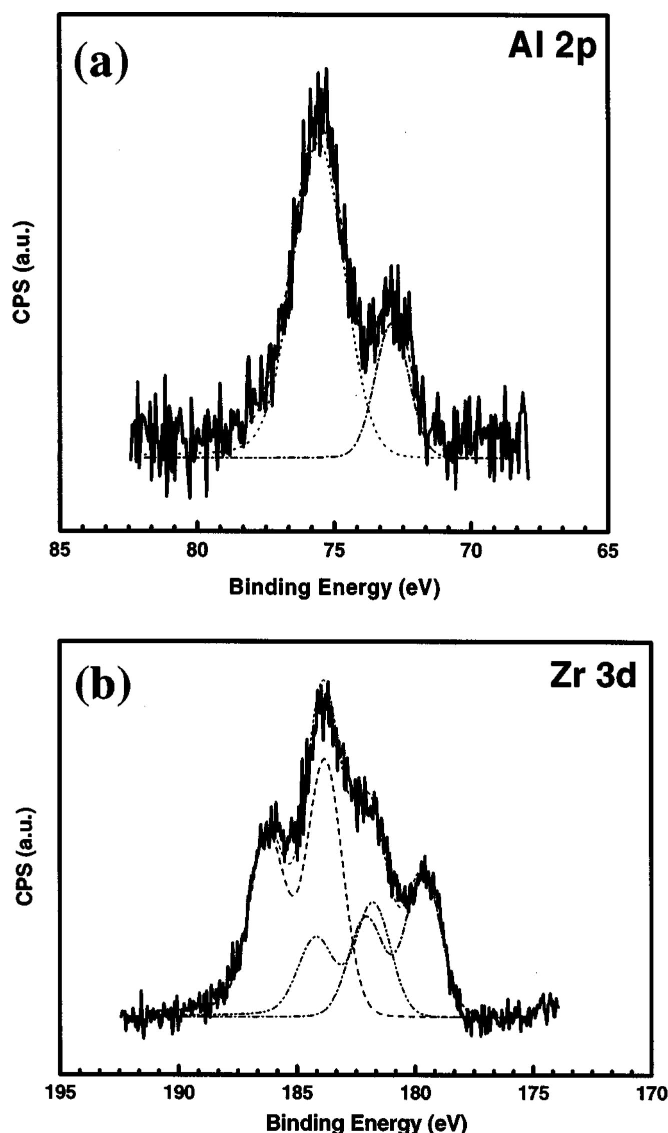

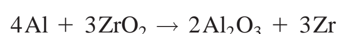

Figure 3. XPS spectra of (a) Al 2p and (b) Zr 3d for ZrO_2 film with Al top electrode at level 4 of the electrode etching process.

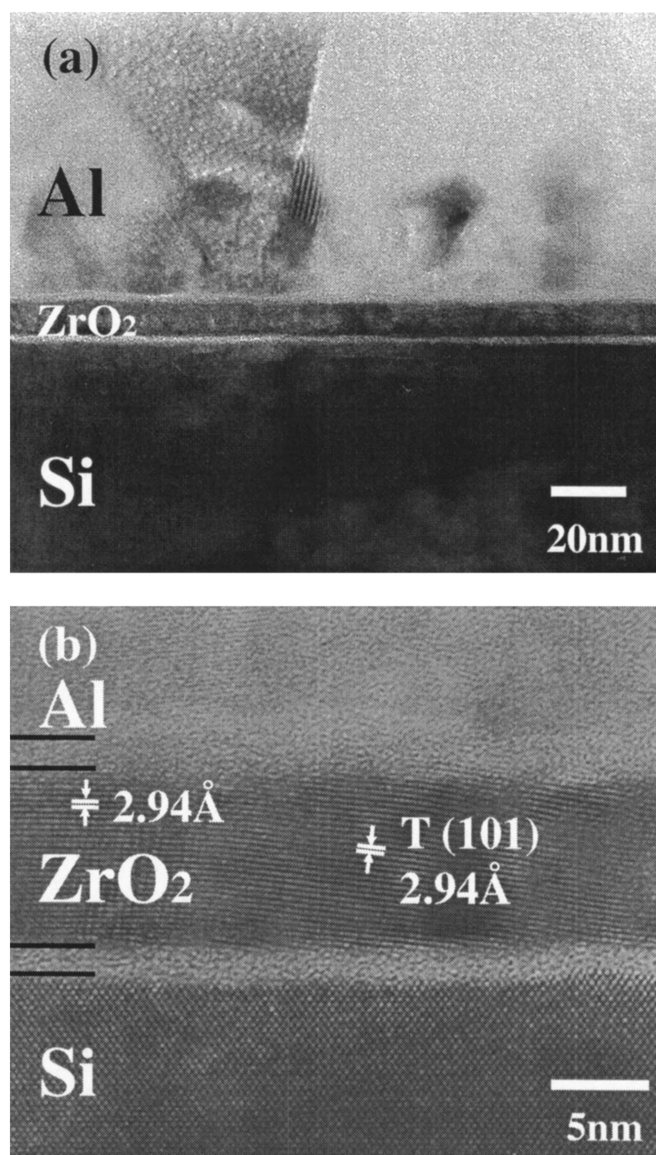

Figure 4. (a) Low-magnification and (b) high-resolution cross-sectional TEM micrographs of ZrO_2 film with Al top electrode.

ence of metallic Al and Al_2O_3 phases.[31] At the same etching stage, the binding energy of Zr $3d_{5/2}$ shows three different peak positions (see Fig. 3b) of 178.9, 181.0, and 183.0 eV, indicating the binding energy of photoelectron characteristics of metallic Zr and ZrO_{2-x} phases at the Al/ZrO_2 interfaces.[31]

Because the chemical reaction on the interface between Al and ZrO_2

$$4Al + 3ZrO_2 \rightarrow 2Al_2O_3 + 3Zr$$

has the negative free energy ($\Delta G_r = -45.37$ kJ/mol at 298 K),[32] Al reduces the top layer of ZrO_2 film into either metallic zirconium or oxygen-deficient zirconia (ZrO_{2-x}) during the deposition of Al. Consequently, the interlayer of the Al-O compound which is presumed to be Al_2O_3 is formed at the Al/ZrO_2 interface. The formation of this interlayer is clearly displayed in the low-magnification TEM micrograph of ZrO_2 film with an Al electrode (Fig. 4a). The HRTEM image in Fig. 4b clearly shows the presence of a 20 Å thick amorphous interlayer, which is presumed to be an Al_2O_3 layer.

In contrast to the Al/ZrO_2 system, the structure with the Pt electrode demonstrated different results. Figure 5 illustrates the evaluation of the Pt 4f signal in XPS spectra as the electrode was etched (level 1 meaning Pt/ZrO_2 and level 6 meaning ZrO_2). In the spectra only peaks with binding energy corresponding to photoelectrons in metallic Pt 4f are observed in all stages of etching. Figure 6a shows the XPS spectra at stage 4, which demonstrated the presence of the Pt $4f_{7/2}$ peak at 71.2 eV. In the same stage, the binding energy of Zr $3d_{5/2}$ is observed only at 183.0 eV, corresponding to that of the stoichiometric ZrO_2 (see Fig. 6b). Such data demonstrate that there is no interaction between the Pt electrode and the ZrO_2 films. Figure 7 shows the cross-sectional TEM micrograph of ZrO_2 film with Pt top electrode in which no interfacial layer is observed between the Pt electrode and ZrO_2 film. Because the free energies for formation of platinum oxides show positive values from thermodynamic consideration,[32] it is more likely that no interfacial layer is formed at the Pt/ZrO_2 interface. In addition, Pt has commonly been used as an electrode because it allows the deposition of dielectric films at high temperature in an oxidizing atmosphere without causing any oxidation of the electrode.

Figure 8 shows the high-frequency C-V characteristics of the ZrO_2 films after annealing in a tube furnace at 600°C for 5 min in an N_2 gas ambient. Al and Pt are deposited as electrodes after annealing

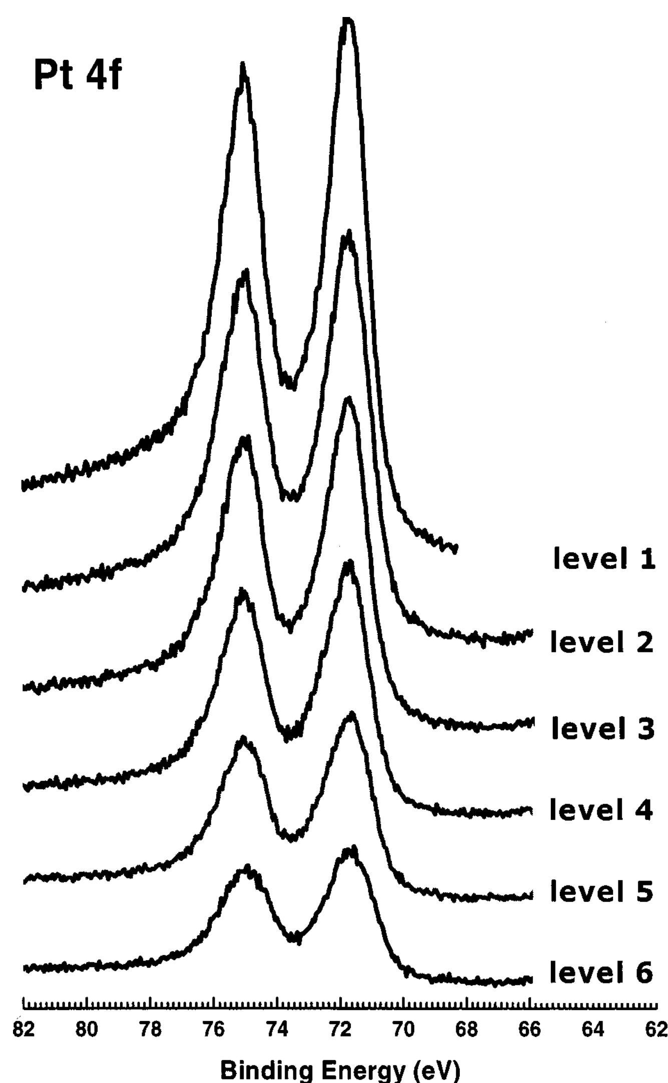

Figure 5. Pt 4f signal in XPS spectra for ZrO_2 film with Pt top electrode.

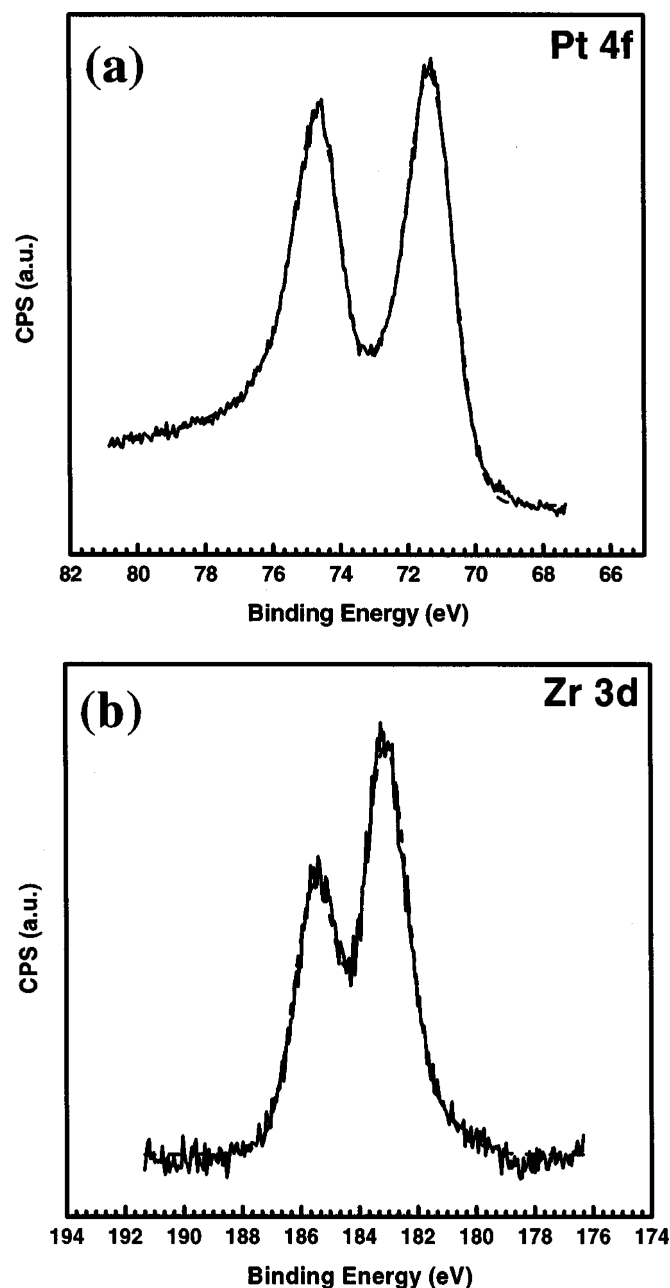

Figure 6. XPS spectra of (a) Pt 4f and (b) Zr 3d for ZrO_2 film with Pt top electrode at level 4 of the electrode etching process.

of ZrO_2 films, and no additional postannealing was performed after the deposition of the electrodes. Although the TEM image indicates the physical thickness of the ZrO_2 film at 9-10 nm in both cases, the measured accumulation capacitance values strongly depend on top electrode materials. CET values extracted from an accumulation capacitance without considering the quantum mechanical effect for the annealed ZrO_2 films with Pt electrode are measured to be about 34.8 Å, which is smaller than 47.2 Å for the one with an Al electrode. This is explained by the presence of the additional amorphous interfacial layer at the Al/ZrO_2 interface. The dielectric constant of the interfacial layer k_i is defined as

$$k_i = k_s(T_i/T_{eq})$$

where T_{eq} is the electrical equivalent thickness for the insulating layer, k_s is the dielectric constant of SiO_2, and T_i is the physical thickness of interfacial amorphous layer. Because the difference in CET values between the two cases is about 12.4 Å and T_i is 20 Å, the calculated k_s value is approximately 6.3, which is close to the dielectric constant value of the interfacial Al_2O_3 layer. In addition, the difference of flatband voltage between films having two kinds of electrodes was observed in Fig. 8. The difference is about 1.2 V, resulting from the work function difference between the two electrodes of Al (4.08 eV) and Pt (5.32 eV).

Conclusion

We investigated the interfacial stabilities of ZrO_2 films with Al and Pt electrodes formed by a magnetron sputtering process upon annealing and consequent changes of their MOS capacitor characteristics. The polycrystalline with both monoclinic and tetragonal ZrO_2 phases was observed by HR-TEM images and plan-view diffraction after postannealing at 600°C. In the case of the ZrO_2 film with an Al electrode, we observed the formation of the interfacial Al_2O_3 layer through XPS and HRTEM analyses. In contrast, the structure with Pt electrode displayed no interfacial layer. The CET value for the ZrO_2 films with Pt electrode was calculated to 34.8 Å, while the value for the films with Al electrode was 47.2 Å. This difference is related to the presence of the interfacial layer in the

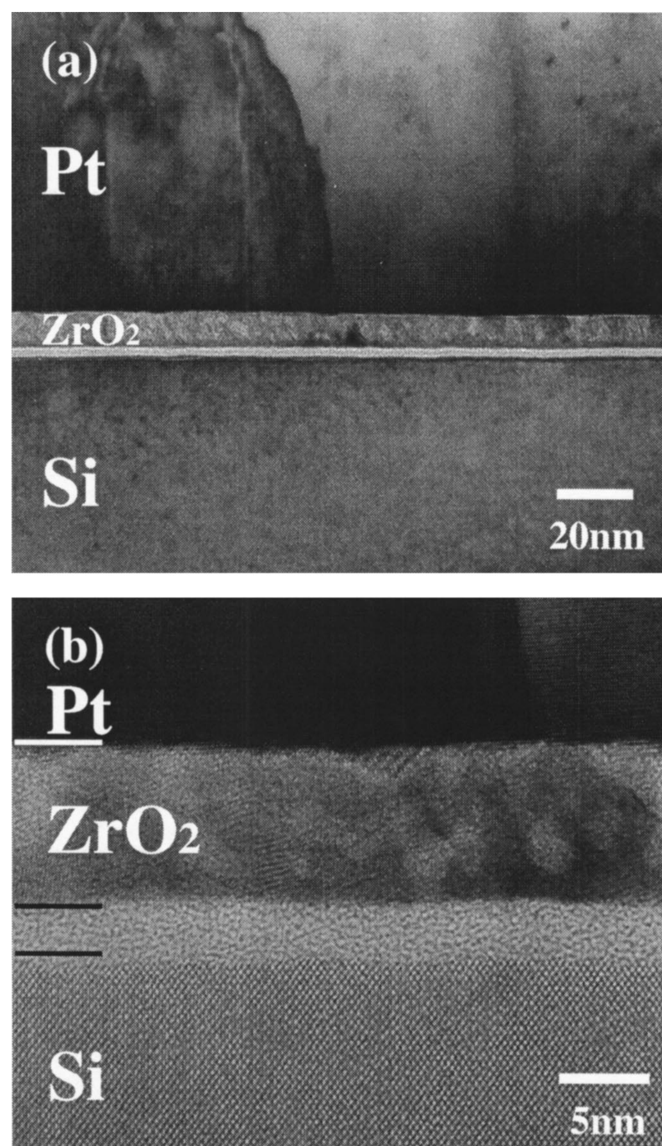

Figure 7. (a) Low-magnification and (b) high-resolution cross-sectional TEM micrographs of ZrO_2 film with Pt top electrode.

Al/ZrO_2 structures. The difference of the flatband voltage (V_{FB}) between $Pt/ZrO_2/Si$ and $Al/ZrO_2/Si$ was about 1.2 V because of their work function differences.

Acknowledgment

This work was partially supported by a scholarship grant from Samsung Electronics Company, Limited, and the Basic Research Program of the Korea Science and Engineering Foundation (Grant No. R01-2001-00271).

Yonsei University assisted in meeting the publication costs of this article.

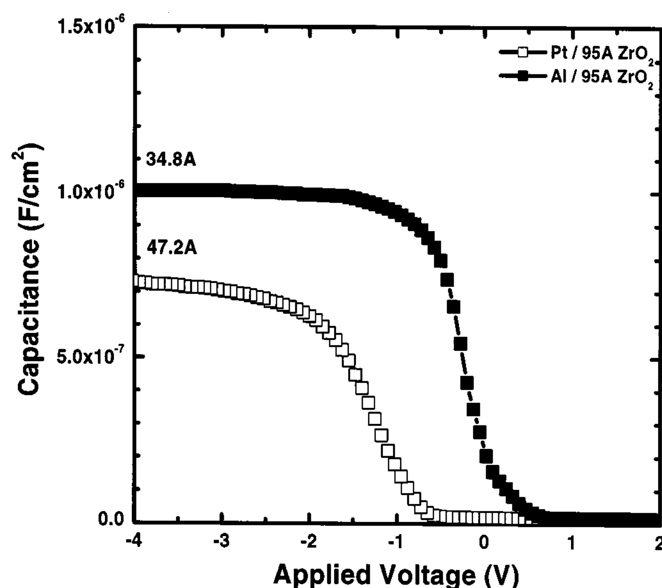

Figure 8. The high-frequency C-V characteristics of Al/ZrO_2/p-Si(100) and Pt/ZrO_2/p-Si(100) diodes.

References

1. L. H. S. Momose, M. Ono, T. Yoshitomi, T. Ohguro, S. Nakamura, M. Saito, and H. Iwai, *IEEE Trans. Electron Devices,* **43**, 1233 (1996).
2. L. B. Cheng, M. Cao, R. Rao, A. Inani, P. Vande Voorde, W. M. Greene, J. M. C. Stork, Z. Yu, P. Zeitzoff, and J. Woo, *IEEE Trans. Electron Devices,* **46**, 1537 (1999).
3. P. M. Zeizoff, *Semiconductor Fabtech*, 10th ed., p. 275, Verteq, Santa Ana, CA (1999).
4. D. Wristers, L. K. Han, T. Chen, H. H. Hwang, and D. L. Kwong, *Appl. Phys. Lett.,* **68**, 2094 (1996).
5. C. Lin, A. I. Chou, K. Kumar, P. Chiudhury, and J. C. Lee, *Appl. Phys. Lett.,* **69**, 1591 (1996).
6. J. Yan, L. K. Han, and D. L. Kwong, *Appl. Phys. Lett.,* **68**, 2666 (1996).
7. M. Cao, P. Vande Voorde, M. Cox, and W. Greene, *IEEE Electron Device Lett.,* **19**, 291 (1998).
8. G. Lucovsky, A. Banerjee, B. Claflin, K. Koh, and H. Yang, *Microelectron. Eng.,* **36**, 207 (1997).
9. S. C. Choi, M. H. Cho, S. W. Whangbo, C. N. Whang, S. B. Kang, S. I. Lee, and M. Y. Lee, *Appl. Phys. Lett.,* **71**, 903 (1997).
10. Y. K. Kim, S. M. Lee, I. S. Park, C. S. Park, S. I. Lee, and M. Y. Lee, *Symposium of VLSI Technology*, p. 52 (1998).
11. H. S. Kim, D. C. Gilmer, and D. L. Polla, *Appl. Phys. Lett.,* **69**, 3860 (1996).
12. S. A. Campbell, D. C. Gilmer, X. Wang, M. T. Hsich, H. S. Kim, W. L. Gladfelter, and J. H. Yan, *IEEE Trans. Electron Devices,* **44**, 104 (1997).
13. K. A. Son, A. Y. Mao, B. Y. Kim, F. Liu, E. D. Pylant, D. A. Hess, J. M. White, D. L. Kwong, D. A. Roberts, and R. N. Vrtis, *J. Vac. Sci. Technol. A,* **16**, 1670 (1998).
14. I. Asano, M. Kunitomo, S. Yamamoto, R. Furukawa, Y. Sugawara, T. Uemura, J. Kuroda, M. Kanai, M. Nakata, and T. Tamaru, *Tech. Dig. - Int. Electron Devices Meet.,* **1998**, 755.
15. Q. Lu, D. Park, A. Kalnitsky, C. Chang, C.-C. Cheng, S. P. Tay, T.-J. King, and C. Hu, *IEEE Electron Device Lett.,* **19**, 341 (1998).
16. P. K. Roy and I. C. Kizilyalli, *Appl. Phys. Lett.,* **72**, 2835 (1998).
17. R. A. Mckee, F. J. Walker, and M. F. Chisholm, *Phys. Rev. Lett.,* **81**, 3014 (1998).
18. H. D. Chen, K. R. Udayakumar, L.E. Cross, J. J. Bernstein, and L. C. Niles, *J. Appl. Phys.,* **77**, 3349 (1995).
19. A. S. Kao, *J. Appl. Phys.,* **69**, 3309 (1991).
20. W. J. Qi, R. Nieh, B. H. Lee, L. Kang, Y. Jeon, K. Onish, T. Ngai, S. Banerjee, and J. C. Lee, *Tech. Dig. - Int. Electron Devices Meet.,* **1999**, 145.
21. M. Copel, M. Gribelyuk, and E. Gusev, *Appl. Phys. Lett.,* **76**, 436 (2000).
22. J. Aarik, A. Aidla, A. A. Kiisler, T. Uustare, and V. Sammelselg, *Thin Solid Films,* **340**, 110 (1999).
23. B. H. Lee, L. Kang, W.-J. Qi, R. Nieh, Y. Jeon, K. Onish, and J. Lee, *Tech. Dig. - Int. Electron Devices Meet.,* **1999**, 145.
24. G. D. Wilk and R. M. Wallace, *Appl. Phys. Lett.,* **74**, 2854 (1999).
25. G. D. Wilk, R. M. Wallace, and J. M. Anthony, *J. Appl. Phys.,* **87**, 484 (2000).
26. K. J. Hubbard and D. G. Schlom, *J. Mater. Res.,* **11**, 2757 (1996).
27. H. Wakabayashi, Y. Saito, K. Takeuchi, T. Mogami, and T. Kunio, *Tech. Dig. - Int. Electron Devices Meet.,* **1999**, 253.
28. S. W. Nam, J. H. Yoo, H. Y. Kim, S. K. Kang, D. H. Ko, C. W. Yang, H. J. Lee, M. H. Cho, and J. H. Ku, *J. Vac. Sci. Technol. A,* **19**, 1720 (2001).
29. J. H. Yoo, S. W. Nam, S. K. Kang, D. H. Ko, and H. J. Lee, *Microelectron. Eng.,* **56**, 187 (2001).
30. S. K. Kang, D. H. Ko, E. H. Kim, M. H. Cho, and C. N. Whang, *Thin Solid Films,* **353**, 8 (1999).
31. *Handbook of X-Ray Photoelectron Spectroscopy*, J. Chastain, Editor, Perkin-Elmer, Eden Prairie, MN (1992).
32. I. Barin and O. Knacke, *Thermochemical Properties of Inorganic Substances*, Springer, New York (1993).